

# DESIGN OF MECHANICAL CLAMPS WITH EXTRA LONG WEDGE GRIPS FOR STATIC AND FATIGUE TESTING OF COMPOSITE MATERIALS IN TENSION AND COMPRESSION

Usually, when performing standard tensile tests, the normal clamps of the tensile machine are ideally suited for the job. However, in some cases, these clamps have some disadvantages.

An important problem occurs when the specimen requires extra space at its ends for special fixtures or sensors. For instance, if the longitudinal strain is measured with an optical fiber sensor,<sup>1–4</sup> this fiber comes out of the specimen at the end (Fig. 1a). Since this fiber breaks off very easily, it requires some space so it can be bent with a relatively large radius. Often, this space is not available.

Another type of in situ monitoring for composites is the use of the carbon fiber-reinforcement for electrical resistance measurement. If the contact electrodes are placed outside the tabs in the strain-free area, as described in references 5–9, sufficient space is required. For example, the setup used in De Baere et al.<sup>9</sup> is illustrated in Fig. 1b, where the gripping of the specimen with standard clamps is shown. The end of the specimen should not touch the clamps because the specimen should be electrically isolated from the tensile machine. In this case, more space should be available. With these clamps, only 35 mm of the available 50 mm of tab length is gripped.

Another problem is that uniaxial testing of composite specimens usually requires tabs on the ends, especially when performing off-axis tests.<sup>10–14</sup> This is also described in the ASTM D3039/D 3039M *Standard Test Method for Tensile Properties of Polymer Matrix Composite Materials*, as well as in the ASTM D 3479/D 3479M *Standard Test Method for Tension-Tension Fatigue of Polymer Matrix Composite Materials*. However, some composites or plastics are not easily bonded, resulting in low ultimate shear stress of the adhesive. By increasing the surface area of the tabs, the fracture load of the specimen can be reached before ultimate shear stress of the adhesive is reached. However, these large tabs still need to fit inside the grips. For example, a carbon fiber-reinforced polyphenylene sulphide (PPS) has an ultimate stress of about 800 MPa. Since PPS is not easily glued, the ultimate shear strength of the adhesive is about 15 MPa or less. By writing the equilibrium in the adhesive layer, the required length of the tabs can be derived as follows:

$$\sigma_{ult}^{specimen} w^{specimen} l^{specimen} = 2\tau_{ult}^{glue} w^{tab} l^{tab} \quad (1)$$

The width of the specimen ( $w^{specimen}$ ) is equal to the width of the tab ( $w^{tab}$ ), a typical thickness of this composite specimen is 2.5 mm. If all these values are implemented in the equation, the tab length is equal to 66.67 mm, which is larger than the average grip length.

All problems above are related to the dimensions of the clamps. In Fig. 2, two types of standard tensile machine fixtures are shown, with the dimensions of grips.

Concerning mechanical grips, the following remarks could be made. If a set of mechanical wedge grips is used, it is usually only suited for either tension or compression testing but rarely for both. For the gripping, the principle of a wedge is used (Fig. 3a). It is obvious that this only works in one direction. If the wedges are pulled down (tensile test), the grips move inwards, increasing contact pressure. However, if the wedges are pushed up (compressive test), the wedges open and the contact pressure decreases. It is possible to have mechanical grips for compressive tests, simply by putting the wedges upside down, but then they will no longer function in tensile conditions.

The problem mentioned above is also present in fatigue loading. Both tension–tension and compression–compression fatigue are possible, using only wedges, but without any other fixture, tension–compression fatigue is impossible. Usually, hydraulic grips (Fig. 2, right) are used for fatigue. These clamps use the wedge principle for tensile mode, whereas the hydraulic plunger supports the grips in compressive mode. However, these clamps still have the problem of insufficient space for extra fixtures and they are expensive. Furthermore, additional hydraulics for the clamps may not always be at hand.

In the next paragraphs, the design of a set of mechanical clamps is presented that can be used for quasi-static and fatigue testing in tension and compression. Furthermore, there is sufficient space for specific fixtures at the ends, for example, optical fibers, contact electrodes, or large tabs.

## DESIGN OF THE CLAMPS

For the design of the clamps, the following specifications must be met:

1. The clamps must be mounted on a servo-hydraulic testing machine to accommodate for fatigue testing.
2. The gripping range of the clamps is 0–12 mm. The average thickness of the composite plates that should be tested on this machine is about 3 mm. However, the thickness may be 11 mm or thicker when tabs are mounted on the specimen, depending on the thickness of the tabs.
3. The load range that the clamps should resist is the same as the load cell, 100 kN in tension and compression, under dynamic loading conditions.

For testing in tension, the principle of a wedge is used (see Fig. 3) as mentioned in the introduction. Therefore, the more the specimen is pulled, the higher the contact pressure becomes and the better the specimen is gripped.

I. De Baere, W. Van Paepegem, and J. Degrieck are affiliated with the Department of Mechanical Construction and Production, Faculty of Engineering, Ghent University, Ghent, Belgium.

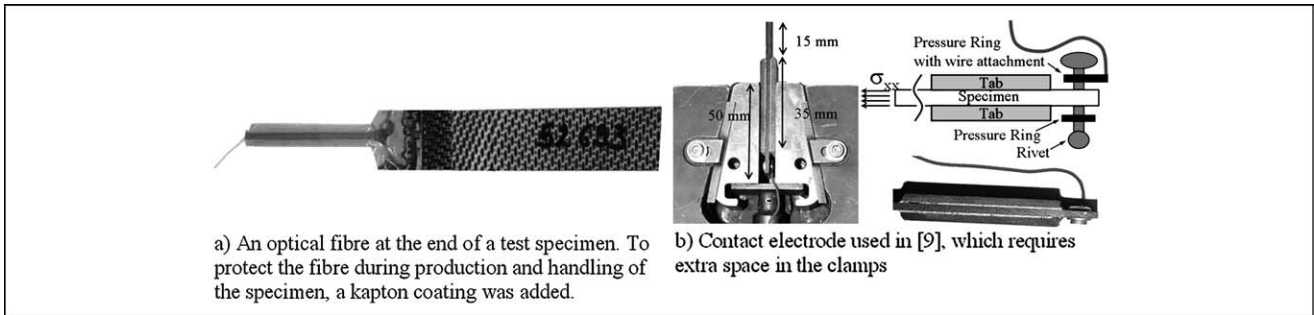


Fig. 1: Two types of extra fixtures required for special sensors

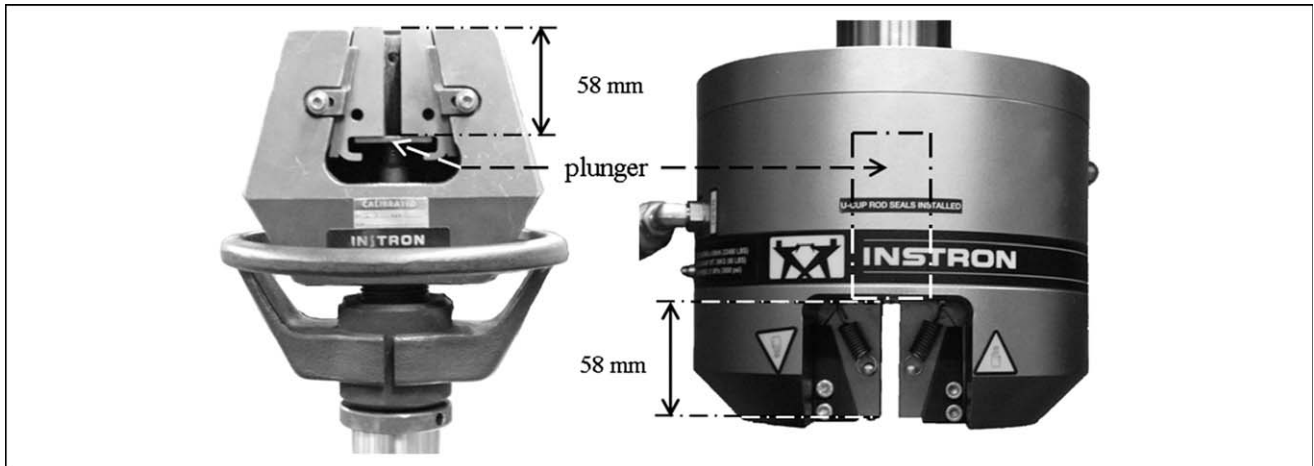


Fig. 2: An illustration of the grip-dimensions of a standard set of mechanical and hydraulic clamps (INSTRON™)

However, the wedge does exactly the opposite when used in compression. An upward motion of the wedge results in a lower contact force. To avoid this, an extra set of horizontal wedges is placed above the wedge-shaped grips (see Fig. 3b).

A certain amount of prestress  $F_V$  is placed on wedge E. This pushes wedge D and both grips downwards, to compensate the upward motion of the grips, caused by the compressive load  $2F$ . Thus, this system has the same function as the hydraulic plunger in the hydraulic clamps (Fig. 2).

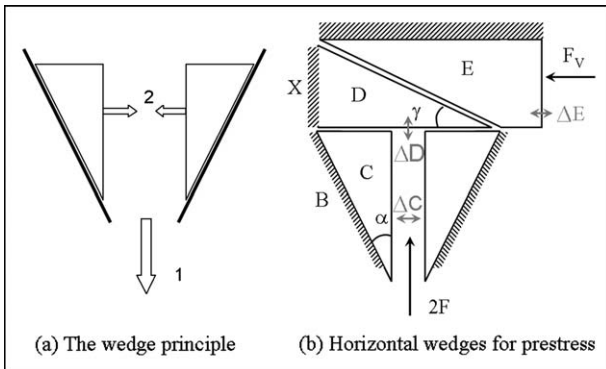


Fig. 3: Illustration of the use of different wedges for the clamp design

The prestress  $F_V$  is provided by a set of disc springs as they can deliver a higher effective force for a twisted springs.

In the next paragraph, the analysis of the influence of the angles  $\alpha$  and  $\gamma$  on the relationship between  $F$  and  $F_V$  is presented.

### Tension after Compression

Initially, the setup in Fig. 4a is considered. Parts D and E are combined in one part (part A), which is considered as a black box. Its function is to deliver a certain downward force on the two grips. The calculation of parts D and E would only complicate the derivation in this stage.

A force of  $2F$  is applied, so that each grip is loaded with  $F$ .

In this analysis, the assumption is made that the clamps will first be loaded in tension and then in compression. This assumption is justified by the fact that a normal tension-compression fatigue test starts in tension. This however has an important influence on the calculation since the loading in tension will put a certain prestress on the clamps that will have an effect when loading in compression afterwards.

In Fig. 4b and c, one grip is illustrated, with all forces that need to be taken into account. The direction of the friction forces  $T_A$  and  $T_B$  is chosen according the way they work.

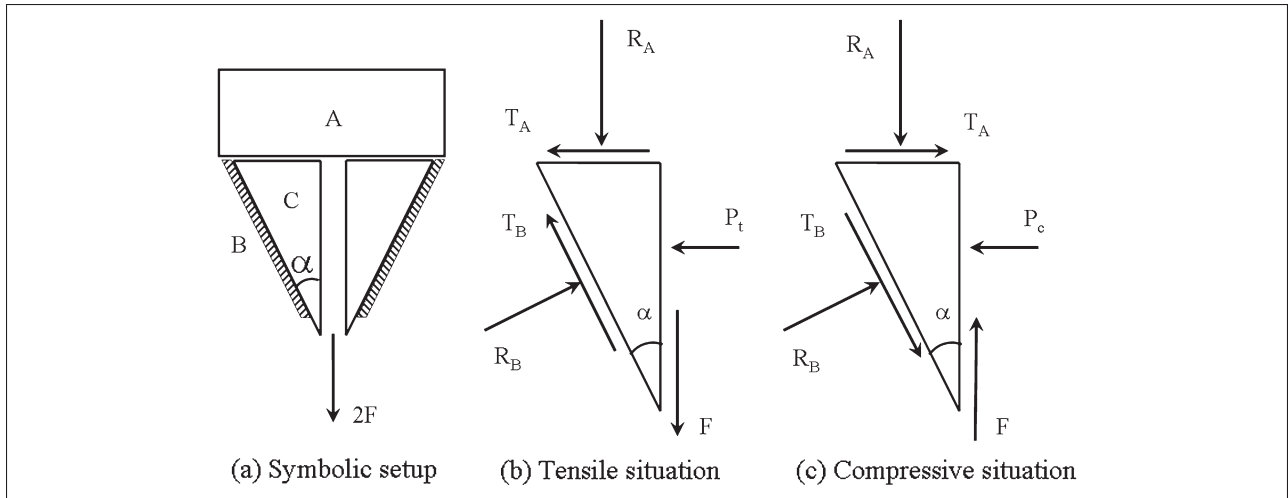


**Fig. 4: Symbolic setup of the design with all reaction forces needed to be taken into account for both the tensile and the compressive situation**

For the tensile situation, the equilibrium of the grip combined with the friction leads to the following equation:

$$\begin{cases} F + R_A = R_B \sin \alpha + T_B \cos \alpha \\ P_t + T_A + T_B \sin \alpha = R_B \cos \alpha \\ T_A \leq \mu_{AC} R_A \\ T_B \leq \mu_{BC} R_B \end{cases} \quad (2)$$

In this equation,  $\mu_{ij}$  is the friction coefficient between parts I and J. In the friction laws, there are ‘less than or equal signs’ because movement only occurs once the tangential force reaches  $\mu$  times the normal force. Once movement occurs, the force needed to sustain the movement is equal to  $\mu$  times the normal force. If the tangential force is lower, no displacement occurs, despite its value.

The worst-case scenario is assumed, which means the maximum value of both  $T_A$  and  $T_B$ . This means exactly before any movement occurs.

This leads to the following:

$$\begin{cases} F + R_A = R_B(\sin \alpha + \mu_{BC} \cos \alpha) \\ P_t + \mu_{AC} R_A + \mu_{BC} R_B \sin \alpha = R_B \cos \alpha \end{cases} \quad (3)$$

From this equation,  $R_B$  can be calculated as follows:

$$R_B = \frac{F + R_A}{\sin \alpha + \mu_{BC} \cos \alpha} \quad (4)$$

With this value, the contact force of the grips on the specimen can be calculated as follows:

$$P_t = F \frac{\cos \alpha - \mu_{BC} \sin \alpha}{\sin \alpha + \mu_{BC} \cos \alpha} + R_A \frac{(1 - \mu_{AC} \mu_{BC}) \cos \alpha - (\mu_{BC} - \mu_{AC}) \sin \alpha}{\sin \alpha + \mu_{BC} \cos \alpha} \quad (5)$$

In this equation, the effect of the wedge is in the first term, and the effect of the prestress is in the second.

Now the compressive situation is considered (Fig. 4c). It is hereby assumed that the force  $R_B$  from Eq. 4 is still present. When the grips are pulled down, the force  $R_B$  has a similar but opposite reaction on part B (Fig. 4a), which symbolizes the clamp. This reaction causes a small elastic deformation of the clamp. When the force  $F$  changes direction (tensile–compressive), this elastic deformation will still be present. Moreover, the friction will inhibit any movement of the parts. Therefore, the reaction  $R_B$  will also remain present. The value of  $R_A$  will also be the same as in the tensile situation.

Equilibrium of the grip combined with the friction laws in Fig. 4c yields the following:

$$\begin{cases} F + R_B \sin \alpha = R_A + T_B \cos \alpha \\ P_c = T_A + R_B \cos \alpha + T_B \sin \alpha \\ T_A \leq \mu_{AC} R_A \\ T_B \leq \mu_{BC} R_B \end{cases} \quad (6)$$

Again, the highest values of  $T_A$  and  $T_B$  are assumed. Together with the known value of  $R_B$  (Eq. 4), this gives for the contact force of the grips on the specimen:

$$P_c = F \frac{\cos \alpha + \mu_{BC} \sin \alpha}{\sin \alpha + \mu_{BC} \cos \alpha} + R_A \frac{(1 + \mu_{AC} \mu_{BC}) \cos \alpha + (\mu_{AC} + \mu_{BC}) \sin \alpha}{\sin \alpha + \mu_{BC} \cos \alpha} \quad (7)$$

Furthermore, the required value of  $R_A$  can be calculated from the first line of Eq. 6:

$$R_A = F + R_B(\sin \alpha - \mu_{BC} \cos \alpha) \quad (8)$$

Since  $R_B$  is known as a function of  $F$  and  $R_A$  (Eq. 4), the amount of prestress  $R_A$  required for a tension–compression

test with amplitude  $2F$  (Fig. 4a) can be determined as a function of  $F$ :

$$R_A = \frac{\tan \alpha}{\mu_{BC}} F \quad (9)$$

It is hereby assumed that the value of  $R_A$  is the same in the tensile and compressive situation. This assumption is justified by the fact that all calculations are done in the situation just before there is any movement of the parts. Since there is no movement, there will be no change in  $R_A$ .

At this point in the calculation, part A can be examined in more detail. A symbolic representation is given in Fig. 5. The objective is to find a value of  $F_V$  as a function of  $F$ .

In Fig. 5, the friction and reaction forces on both wedges are given. By writing equilibrium, a relationship between  $R_A$  and  $F_V$  can be found, and since the relationship between  $R_A$  and  $F$  is known, an equation for  $F_V$  as a function of  $F$  can be derived.

The equilibrium of part D yields the following:

$$\begin{cases} 2R_A = T_X + N_E \cos \gamma + T_E \sin \gamma \\ N_X + T_E \cos \gamma = N_E \sin \gamma \\ T_E \leq \mu_{DE} N_E \\ T_X \leq \mu_{DX} N_X \end{cases} \quad (10)$$

As before, the moment just before movement is considered, which means the maximum values of  $T_E$  and  $T_X$  are chosen. Thus, a value for  $R_A$  can be calculated as follows:

$$R_A = \frac{1}{2} N_E [(1 - \mu_{DE} \mu_{DX}) \cos \gamma + (\mu_{DE} + \mu_{DX}) \sin \gamma] \quad (11)$$

The equilibrium of part E gives the following:

$$\begin{cases} F_V + T_Y + T_E \cos \gamma = N_E \sin \gamma \\ N_Y = N_E \cos \gamma + T_E \sin \gamma \\ T_E \leq \mu_{DE} N_E \\ T_Y \leq \mu_{EY} N_Y \end{cases} \quad (12)$$

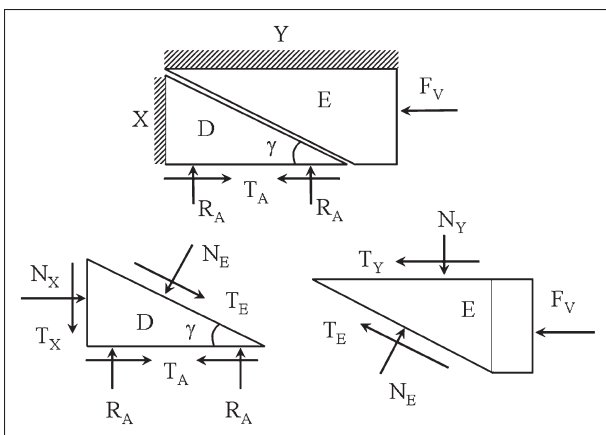


**Fig. 5: Symbolic representation of the part that imposes the prestress  $R_A$  with all (reaction) forces on the wedges illustrated**

Again with the maximum values of  $T_E$  and  $T_Y$ , the formula for  $F_V$  can be derived by the following:

$$F_V = N_E [(1 - \mu_{DE} \mu_{EX}) \sin \gamma - (\mu_{DE} + \mu_{EX}) \cos \gamma] \quad (13)$$

The expression for  $N_E$  can be calculated using Eq. 11. Combining this with the previous equation and Eq. 9, the following relation between the load  $F$  and the needed prestress  $F_V$  is found:

$$F_V = 2 \tan \alpha \frac{1 - \mu_{DE} \mu_{EX} \sin \gamma - (\mu_{DE} + \mu_{DX}) \cos \gamma}{\mu_{BC} (1 - \mu_{DE} \mu_{EX}) \cos \gamma + (\mu_{DE} + \mu_{DX}) \sin \gamma} F \quad (14)$$

In this equation,  $\mu_{ij}$  is the coefficient of friction between parts I and J.

Since these friction coefficients are only known within a relatively large margin, all coefficients are chosen equal to 0.1. Normally, the friction coefficient between steel and steel is about 0.6, but to avoid micro-welding of the metal surfaces, a special coating is used and some parts are greased. Both precautions lower the friction coefficient. With these values of  $\mu_{ij}$ , the equation becomes the following:

$$f = \frac{F_V}{2F} = \tan \alpha \frac{990 \sin \gamma - 200 \cos \gamma}{99 \cos \gamma + 20 \sin \gamma} \quad (15)$$

It can be concluded that an increase in  $\gamma$  or in  $\alpha$  gives an increase in  $f$ , which means a stronger spring will be necessary. Therefore, a low value of both angles is preferred.

It may also be noticed that the ratio becomes zero for a value of  $\gamma$  of  $11.4^\circ$ . A negative value means that  $F_V$  changes direction in Fig. 3b. This is actually a consequence of the used model. In the deduction of Eq. 14, the maximum values of the tangential forces ( $T_A, T_B, T_E, \dots$ ) were chosen. In reality, when the model predicts a negative value for  $F_V$ , this would mean that the friction between all parts is large enough to carry the load.

In order to choose the values of  $\alpha$  and  $\gamma$ , not only the force  $F_V$  but also the gripping of the specimen itself needs to be taken under consideration. Figure 3b gives an overview of the movement of all parts in the design.  $\Delta E$  is the displacement of the prestress setup that is imposed by the user and  $\Delta C$  is the narrowing of the grips as a consequence of  $\Delta E$ . The purpose is to have a relatively large  $\Delta C$  with a relatively small  $\Delta E$  in order to keep the dimensions of the parts reasonable.

Some simple trigonometry gives the following:

$$\begin{cases} \Delta D = \Delta E \tan \gamma \\ \Delta C = 2 \Delta D \tan \alpha \end{cases} \Rightarrow \Delta C = 2 \Delta E \tan \alpha \tan \gamma \Rightarrow \frac{\Delta C}{\Delta E} = 2 \tan \alpha \tan \gamma \quad (16)$$

It can be concluded that an increase in  $\alpha$  or  $\gamma$  gives an increase in the displacement ratio. This means that a high

value of the angles is preferable because otherwise, more horizontal space is required inside the clamps for part E to move (Fig. 3b).

Both  $\alpha$  and  $\gamma$  also have an effect on the geometry of the clamps. The smaller  $\alpha$  is, the longer the grips become, resulting in more space for extra fixtures on the specimen. The larger  $\gamma$  becomes, the higher the wedge system (parts D and E in Fig. 3b), which increases the height of clamps and as a result the total weight of the clamps. The latter results in not only higher forces of inertia during a test but also gives more difficulty in mounting the clamps. Therefore, the angles should be chosen sufficiently small.

Finally, a compromise was chosen between a high value for the displacement and a low value for the springs, taking the effect of the angles on the geometry into account. Values of  $10^\circ$  for the grips and  $20^\circ$  for the wedges were chosen. With these angles, it is possible to calculate the force  $F_V$  necessary to compensate a total compressive force  $F_{tot}$  equal to  $2F$ , using Eq. 14.

$$F_V = 0.266F_{tot} \quad (17)$$

The clamps should resist a dynamic load of 100 kN, resulting in an  $F_V$  of 26.6 kN. Two disc springs of 15 kN are placed in series, resulting in a total force of 30 kN. Six of these sets are placed in parallel, in order to regulate the prestress. One set of discs reaches 30 kN after an deflection of 1.05 mm. With six sets of discs, there is 6.3 mm of displacement ( $\Delta E$ ) available to reach the 30 kN.

**Clamps Only Loaded in Compression**

In the paragraph above, compression after tension is considered. But what happens with tests in compression–compression, where there is no tension to preload the clamps? In this paragraph, the calculation is done for the worst-case scenario: compression without any form of preloading of the clamps.

A few things change when the clamps are immediately loaded in compression, which is the case with a quasi-static compression test or compression–compression fatigue. In this scenario, all prestress of the clamps is lost and the wedges

need to compensate the entire load. This gives the following formula instead of Eq. 9:

$$R_A = F \quad (18)$$

This indicates that

$$\frac{\tan \alpha}{\mu_{BC}} = 1 \quad (19)$$

Substituting this in Eq. 14 gives the following:

$$\frac{F_V}{2F} = \frac{(1 - \mu_{DE}\mu_{EX})\sin \gamma - (\mu_{DE} + \mu_{DX})\cos \gamma}{(1 - \mu_{DE}\mu_{EX})\cos \gamma + (\mu_{DE} + \mu_{DX})\sin \gamma} \quad (20)$$

With the values of  $\mu_{ij}$  equal to 0.1,  $\alpha$  equal to  $10^\circ$  and  $\gamma$  equal to  $20^\circ$ , this ratio becomes the following:

$$F_V = 0.151F_{tot} \quad (21)$$

This means that the preload, given by the disc springs, is even lower in this case than it was in tension–compression. This can be explained by the absence of the effect of  $R_B$  on  $R_A$ . Therefore, the disc springs, selected in the paragraph above, are sufficient.

**Space for Extra Fixtures?**

Given the principle illustrated in Fig. 3b, it is clear that the only location where extra space can be created is between the grips. Therefore, the grips are chosen extra long, which also ensures that long end tabs can be gripped. The housing of the grips (part B in Fig. 3b) is therefore widened. This is illustrated in Fig. 6. If the housing is broadened over a distance  $d$ , the length of the grips increases from  $l$  to  $L$ .

Since the sandwich load cell of our servo hydraulic testing machine had six M20 holes in a circle with a diameter of 150 mm, the clamps were designed as a cylinder with a diameter of 200 mm, with holes so large that long M20 bolts can be mounted through the cylinder.

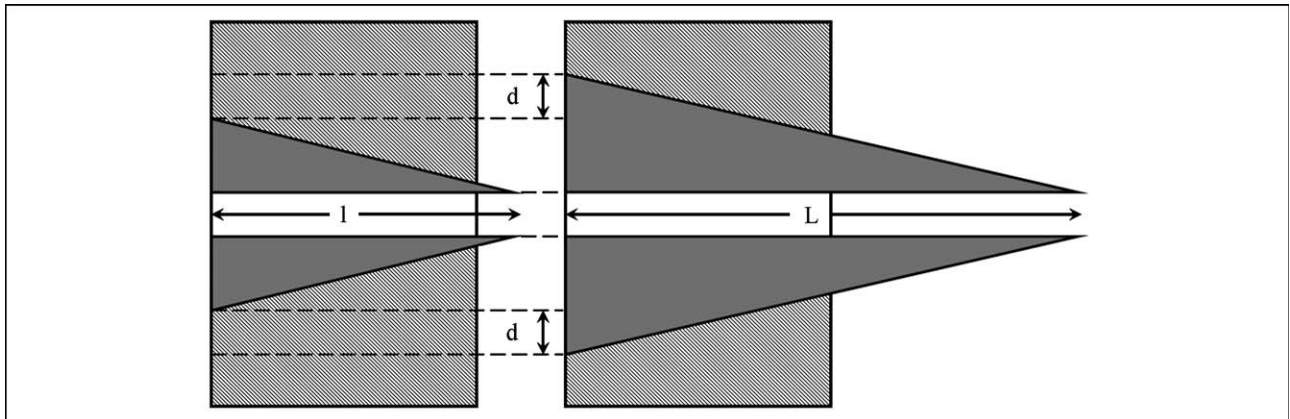


**Fig. 6:** Illustration of the effect of the widening of the housing of the grips

The final design of the clamps is given in Fig. 7.

The wedge system (2), which represents parts D and E in Fig. 5, pushes the two long grips (1) down. The top wedge is connected with the preload system (4, 5, and 6) by a bolt (3). The preload is delivered by six sets of disc springs (4), which were discussed in a previous paragraph. These springs are able to move between the head of bolt (6) and the head of bolt (3). To guide the springs over the bolt (3), a small cylinder (5) is used. This cylinder can also regulate the preload: a different length gives a different indentation of the springs and as a result a different preload. A hollow bolt (6) screws in the cylinder and runs over bolt (3). Its head makes contact with the last disc spring. Two long bolts (7) are there to prevent the bottom from opening when large loads are applied. Finally, discs with different thicknesses (8) are used to regulate the distance between the grips. For the range 0–10 mm, there are five setups with a small overlap between ranges, to make it user-friendly.

Once the correct disc is chosen, a specimen can be mounted: bolt (6) is screwed out of the cylinder, which causes parts 3, 4, and 5 and the top wedge to move to the left. This results in the downward motion of the bottom wedge and both grips (1). Once these grips make contact with the specimen, the preload is placed on the system by further screwing out bolt (6). This causes a certain indentation of the disc springs, resulting in the preload.

**Finite-Element Modelling of the Cylinder**

For the design, the drawing package ‘Solidworks 2003’ was used. In this package, there is also a finite elements module, ‘COSMOS Express’, that was used to determine the stress distribution in the cylinder.

In order to ensure an infinite fatigue life under loading of 100 kN, a safety factor of 3 with respect to the yield stress was taken into account when designing the cylinder. Because of the high loads, a high-strength steel was chosen. For the simulation, done with the COSMOS express package, the following material constants were used (Table 1).

Applying a load of 100 kN in tension results in Fig. 8, where the values of the Von Mises criterium are illustrated, the deformation is scaled with a factor of 598.

The minimum factor of safety is 6.66, which means a maximum stress of 93.1 MPa when applying the maximum load of 100 kN. This should ensure infinite fatigue life.

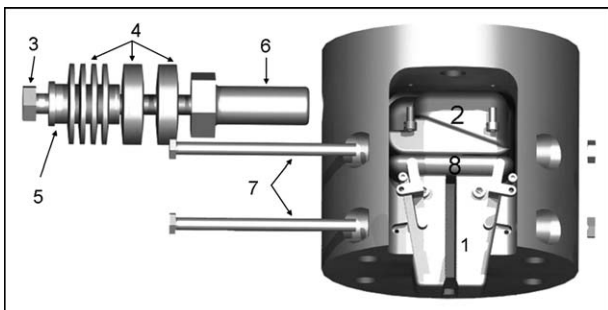


**Fig. 7: Exploded view of the clamps for tension and compression fatigue loading**

**Table 1—The used material constants in COSMOS express**

Elastic modulus	210,000 MPa
Poisson's ratio	0.28
Yield strength	620 MPa
Mass density	7700 kg/m <sup>3</sup>

The mechanical clamps were made out of two steels: the THYROPLAST 2311 and the THYROPLAST 3344 EFS. The former is a quenched and tempered steel with a supplied hardness of 280–325 HB. However, hardness and strength can still be modified by thermal treatment. This was done in order to achieve a material with a hardness of 51 Rockwell Hardness on Scale C (HRC) and a tensile strength of 1730 MPa. The material has no yield strength; the behavior is linear until fracture. The DIN material number is 1.2311 and it is referred to as 40 CrMnMo 7.

The THYROPLAST 3344 EFS is also a quenched and tempered steel, but with a different chemical composition, resulting in a better toughness and tensile strength. After quenching, the material has a hardness of 54 HRC and a tensile strength of 1910 MPa. The DIN material number is 1.2344 and is referred to as X 40 CrMoV 5 1. This material was recommended for the highest demands.

The cylinder, the grips, the hollow bolt (item (6) in Fig. 7), and the fixing medium for the tensile machine have been produced with the THYROPLAST 2344 since these parts are subjected to the highest (fatigue) loads. All other parts have been manufactured in THYROPLAST 2311.

After production, the cylinders were nitrited for a higher surface hardness since thermal hardening would result in large, intolerable deformations. The other parts are coated with a (black) nitride layer with a ‘niblox’ treatment to avoid micro-welding of the surfaces.

A detailed image of the clamp is shown in Fig. 9.

With these clamps, several static and fatigue experiments were performed in tension and compression. The clamps do not seem to have any demonstrable influence on the derived results, such as in-plane elastic properties and fatigue lifetime. Furthermore, the manufacturing of the clamps cost about one third the price of commercial hydraulic clamps.

**FINITE-ELEMENT VERIFICATION OF THE CONTACT PRESSURE**

In order to have a verification of the theoretical deduction in the previous paragraphs, a simulation of a part of the mechanism has been done with the finite element package ABAQUS™/Standard v6.6-2. The purpose of this simulation is to verify if Eq. 5 is accurate.

Two simulations were performed, one with  $\mu$  equal to 0.1 and one with  $\mu$  equal to 0, which means no friction occurred.

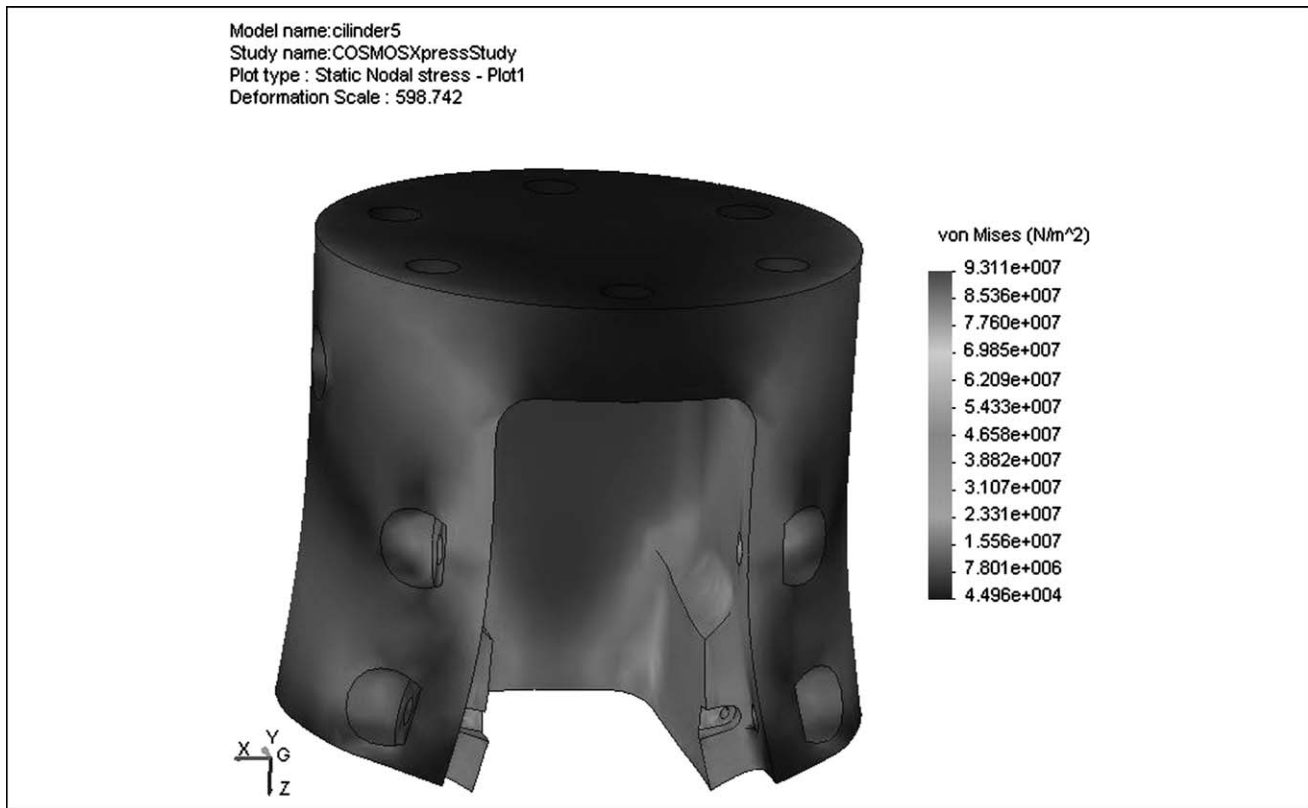


**Fig. 8: Von Mises stress distribution in the cylinder when applying a load of 100 kN. Deformation factor is 598; maximum stress level is 93.1 MPa**

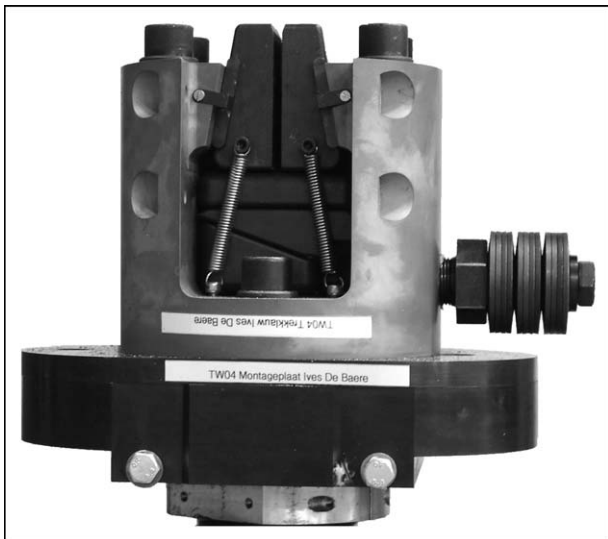


**Fig. 9: Detail of the clamp**

Values for  $R_A$  and  $F$  can be derived from the simulation. With both values, an average contact pressure  $p_t$  can be calculated using Eq. 5 and by dividing the contact force  $P_t$  by the surface of the contact area between tab and specimen.

For comparison, an average contact pressure for the ABAQUS simulation is calculated by integrating the local contact pres-

**Table 2—Results of both the ABAQUS simulation and the prediction with the derived model**

Friction coefficient $\mu$ (—)	0.0	0.1
Force $F$ (kN)	17.89	16.43
Force $R_A$ (kN)	3.78	18.09
Averaged $P_t$ (ABAQUS) (MPa)	67.33	66.97
Predicted $P_t$ (model) (MPa)	68.26	68.45

sure over the surface, yielding a resultant force, and dividing this resultant force by the surface of the tab  $A_{tab}$ . An overview of both simulations is given in Table 2.

It may be concluded that the theoretical model predicts the actual value very well.

## CONCLUSIONS

Based on the results obtained in the previous paragraphs, the following conclusions may be drawn:

- It is possible to design a set of mechanical clamps with extra long wedge grips, used for tension–compression fatigue without influencing fatigue lifetime.
- The design allows the use of long tabs or any other fixtures at the end of the specimen, for example, optical fibers or contact electrodes for electrical resistance measurement.

- The proposed setup does not have any influence on the mechanical and tensile properties of the tested material in static tensile testing.
- The contact pressure, predicted by the derived model corresponds excellently with the results from the ABAQUS simulation of the clamps.

## ACKNOWLEDGMENT

The authors are highly indebted to the university research fund BOF (Bijzonder Onderzoeksfonds UGent) for sponsoring this research.

## References

1. De Waele, W., Degrieck, J., De Baets, P., Moerman, W., and Taerwe, L., "Feasibility of Integrated Optical Fibre Sensors for Condition Monitoring of Composite Structures—Part II: Combination of Bragg-sensors and Acoustic Emission Detection," *Insight* **45**(8): 542–553 (2003).
2. De Waele, W., Degrieck, J., Baets, R., Moerman, W., and Taerwe, L., "Load and Deformation Monitoring of Composite Pressure Vessels by Means of Optical Fibre Sensors," *Insight* **43**(8): 518–525 (2001).
3. Shin, C.S., and Chiang, C.C., "Fatigue Damage Monitoring in Polymeric Composites Using Multiple Fiber Bragg Gratings," *International Journal of Fatigue* **28**(10):1315–1321 (2006), The Third International Conference on Fatigue of Composites.
4. Sorensen, L., Gmür, T., and Botsis, J., "Residual Strain Development in an AS4/PPS Thermoplastic Composite Measured Using Fibre Bragg Grating Sensors," *Composites Part A: Applied Science and Manufacturing* **37**(2):270–281 (2006).
5. Seo, D.C., and Lee, J.J., "Damage Detection of CFRP Laminates Using Electrical Resistance Measurement and Neural Network," *Composite Structures* **47**(1–4):525–530 (1999).
6. Angelidis, N., Wei, C.Y., and Irving, P.E., "The Electrical Resistance Response of Continuous Carbon Fibre Composite Laminates to Mechanical Strain," *Composites Part A—Applied Science and Manufacturing* **35**(10):1135–1147 (2004).
7. Park, J.B., Okabe, T., and Takeda, N., "New Concept for Modelling the Electromechanical Behavior of Unidirectional Carbon-fiber-reinforced Plastic Under Tensile Loading," *Smart Materials and Structures* **12**(1):105–114 (2003).
8. Irving, P.E., and Thiagarajan, C., "Fatigue Damage Characterization in Carbon Fibre Composite Materials Using an Electrical Potential Technique," *Smart Materials and Structures* **7**(4):456–466 (1998).
9. De Baere, I., Van Paepegem, W., and Degrieck, J., "The Use of Rivets for Electrical Resistance Measurement on Carbon Fibre-reinforced Thermoplastics," *Submitted to Smart Materials and Structures*.
10. Van Paepegem, W., De Baere, I., and Degrieck, J., "Modelling the Nonlinear Shear Stress-strain Response of Glass Fibre-reinforced Composites. Part I: Experimental Results," *Composites Science and Technology* **66**:1455–1464 (2006).
11. Sun, C.T., and Chung, I., "An Oblique End-tab Design for Testing Off-axis Composite Specimens," *Composites* **24**(8):619–623 (1993).
12. Pierron, F., and Vautrin, A., "The 10deg Off-axis Tensile Test: A Critical Approach," *Composites Science and Technology* **56**: 483–488 (1996).
13. Pierron, F., and Vautrin, A., "New Ideas on the Measurement of the In-plane Shear Strength of Unidirectional Composites," *Journal of Composite Materials* **31**(9):889–895 (1997).
14. Pierron, F., Alloba, E., Surrel, Y., and Vautrin, A., "Whole-field Assessment of the Effects of Boundary Conditions on the Strain Field in Off-axis Tensile Testing of Unidirectional Composites," *Composites Science and Technology* **58**:1939–1947 (1998). ■